Magnetic Resonance Imaging 63 (2019) 185–192

Contents lists available at ScienceDirect

Magnetic Resonance Imaging

journal homepage: www.elsevier.com/locate/mri

Original contribution

Region-of-interest undersampled MRI reconstruction: A deep convolutional neural network approach

Liyan Sun[a], Zhiwen Fan[a], Xinghao Ding[a,*], Yue Huang[a], John Paisley[b]

[a] Fujian Key Laboratory of Sensing and Computing for Smart City, Xiamen University, Fujian, China
[b] Department of Electrical Engineering, Columbia University, New York, NY, USA

ARTICLE INFO

Keywords:
Deep convolutional neural network
Magnetic resonance imaging
Image reconstruction
Region of interest

ABSTRACT

Compressive sensing enables fast magnetic resonance imaging (MRI) reconstruction with undersampled k-space data. However, in most existing MRI reconstruction models, the whole MR image is targeted and reconstructed without taking specific tissue regions into consideration. This may fails to emphasize the reconstruction accuracy on important and region-of-interest (ROI) tissues for diagnosis. In some ROI-based MRI reconstruction models, the ROI mask is extracted by human experts in advance, which is laborious when the MRI datasets are too large. In this paper, we propose a deep neural network architecture for ROI MRI reconstruction called ROIRecNet to improve reconstruction accuracy of the ROI regions in under-sampled MRI. In the model, we obtain the ROI masks by feeding an initially reconstructed MRI from a pre-trained MRI reconstruction network (RecNet) to a pre-trained MRI segmentation network (ROINet). Then we fine-tune the RecNet with a binary weighted ℓ_2 loss function using the produced ROI mask. The resulting ROIRecNet can offer more focus on the ROI. We test the model on the MRBrainS13 dataset with different brain tissues being ROIs. The experiment shows the proposed ROIRecNet can significantly improve the reconstruction quality of the region of interest.

1. Introduction

Magnetic resonance imaging (MRI) is a medical imaging modality that generates high-resolution anatomical images with little radiation, but is potentially limited by slow data acquisition speed [1]. Different acceleration techniques have been proposed such as fast pulse sequence designs, parallel imaging, and applying compressed sensing theory. Compressed sensing has attracted researchers' attention in general because of the wide applicability of its theory, which proves a signal can be very accurately recovered with few measurements if it can be sparsely represented [2]. Compressed sensing methods have been explored in fast MR imaging (CS-MRI) for acceleration and are recently being employed by industry [3].

In conventional MRI reconstruction methods built upon compressed sensing, a reconstructed image is produced based on interpolating the unsampled Fourier measurements in k-space. The classic CS-MRI problem can be formulated as

$$x = \underset{x}{\operatorname{argmin}} \ \|F_u x - y\|_2^2 + \rho(x), \tag{1}$$

where $x \in \mathbb{C}^{P\times 1}$ is the underlying P-dimensional vectorized MR image and $y \in \mathbb{C}^{Q\times 1}$ ($Q \ll P$) is the under-sampled Q-dimensional k-space measurements with much lower dimension. The undersamped Fourier encoding matrix is denoted as $F_u \in \mathbb{C}^{Q\times P}$. By under-sampling k-space measurements, the imaging can be significantly accelerated. The first term is the data fidelity and second term a regularization. In this objective, $\rho(x)$ encodes the prior information on the desired property of the MRI. The optimization of the problem seeks to minimize the data fidelity loss and regularization loss simultaneously. Conventionally, the sparse priors are used to constrain the ill-posed problem like ℓ_1 norm [4], but recently, deep convolutional neural networks have been utilized to address the problem [5, 6]. Wavelet sparsity and total variation [1, 4] are common fixed-basis regularizers ($\rho(x)$ in Eq. (1)). Some adaptive-basis variants of wavelets [7] or dictionary learning techniques [8, 9] are also used. Recently, deep neural networks have been applied to undersampled MRI reconstruction [10], achieving state-of-the-art performance in both quality and efficiency.

From the objective in Eq. (1), it is worth noting that all the pixels in the MR image x are typically weighted equally, regardless of the specific tissues. In other words, conventional MRI reconstruction methods lack the ability to provide better reconstruction quality a region of interest (ROI). However, in real application scenarios, different tissues in the same MRI represents different biological information, and in some cases the needs to focus on certain tissues over others exists. For

* Corresponding author.
E-mail address: dxh@xmu.edu.cn (X. Ding).

https://doi.org/10.1016/j.mri.2019.07.010
Received 23 March 2019; Received in revised form 6 July 2019; Accepted 14 July 2019

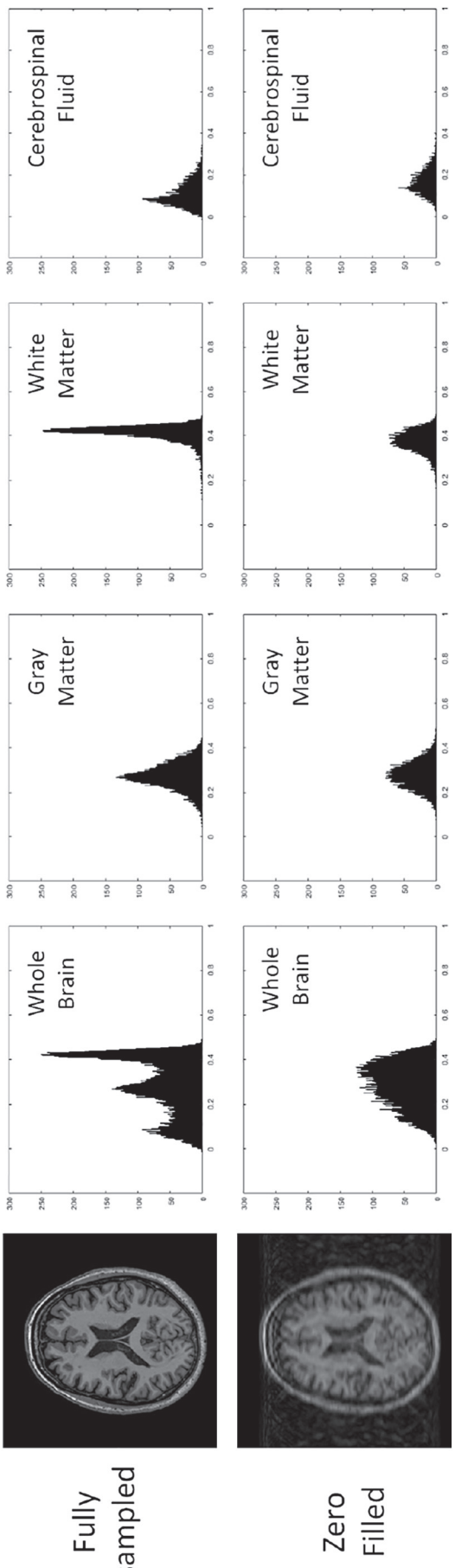

Fig. 1. The histograms of one brain image and the tissues with fully-sampled and zero-filled.

example, white matter lesions are closely related to Alzheimer disease and appears in the white matter region [11]. The rationale for an ROI strategy is that the specific tissue of interest usually contains less variation compared with the entire image, which makes learning a function mapping much easier for the deep network. To further illustrate this, we show histograms of an example brain data in Fig. 1. The x-axis of the histograms represents the pixel value and the y-axis denotes how many pixels fall into this intensity value. We observe the histogram of fully-sampled MRI is a complex multimodal distribution corresponding to the different intensity values in the GM, WM and CSF tissues with backgrounds excluded. However, the histogram of zero-filled MRI under-sampled by 20% 1D Cartesian mask shows the obviously different shape compared with fully-sampled one, which is caused by the subsampling in k-space leading to the aliasing artifacts in spatial domain. Thus, learning the mapping from the distribution of zero-filled MRI to complex multi-mode distribution of fully-sampled MRI directly is relatively difficult. To validate the benefit of partitioning the whole brain regions into different semantic regions, we show the histograms of GM, WM and CSF tissue of both fully-sampled and zero-filled MRI. We observe, for each tissue, the distributions of fully-sampled and zero-filled MRI are both regular unimodal distribution. Learning a mapping in the region-of-interest tissue regions can be simplified by such a consistency in distribution shape. Thus our region-of-interest rapid MRI reconstruction approach can produce more accurately reconstructed ROI tissues because function mapping is simplified. Better reconstruction in such regions can improve the confidence of diagnosis. Thus designing a fast task-driven region-of-interest MRI reconstruction framework can provide doctors with more information on specific tissues of interest.

In the work of ROICS [12], an ROI strategy is proposed to better reconstruction the specific tissues. In the method, the ROI is selected manually by human experts. It is then represented as a binary mask $M \in \mathbb{C}^{P\times P}$ and a new ROI objective function is created

$$x = \underset{x}{\operatorname{argmin}} \ \|MF_u^H(F_u x - y)\|_2^2 + \lambda \ \|\Psi(Mx)\|_1, \tag{2}$$

where Ψ is a sparsity-inducing transform operator. We note that this objective function is designed to focus on the specific regions selected manually in advance. A similar idea is adopted in the user-guided compressed sensing magnetic resonance angiography (CS-MRA) [13, 14], where the angiography is relatively small compared with the background meaning equal weight on all pixels would cause the angiography to be less emphasized. A method based on region growing was used by [15]. Although the reconstruction accuracy region-of-interest tissues is promoted, the ROI masks are determined manually in advance by human expert. To relieve the increased human burden brought by laborious manual labeling when handling massive medical data, fully automatic medical image segmentation algorithm is a suitable approach to obtain region-of-interest masks.

Automatic segmentation algorithms do pixel-level classification to divide an image into different regions. In medical image analysis, automatic MRI segmentation algorithms are developed to distinguish different tissues and help focus localization. Conventionally, segmentation algorithms are based on a region growing strategy [16], which lacks semantic information that can lead to unsatisfactory segmentation. Other segmentation models are based on atlas methods [17], requiring accurate registration and heavy computation. Classic machine learning methods like random forest combined with hand-crafted features are also used for segmentation [18]. Recently, deep neural networks have been adapted to MRI segmentation [19, 20] with good results.

In this paper, we proposed a region-of-interest undersampled MRI reconstruction model called ROIRecNet based on a deep neural network. We first pre-train a deep convolutional neural network called (RecNet) for MRI reconstruction using zero-filled and fully-sampled MRI training pairs. We also train a deep network for MRI segmentation

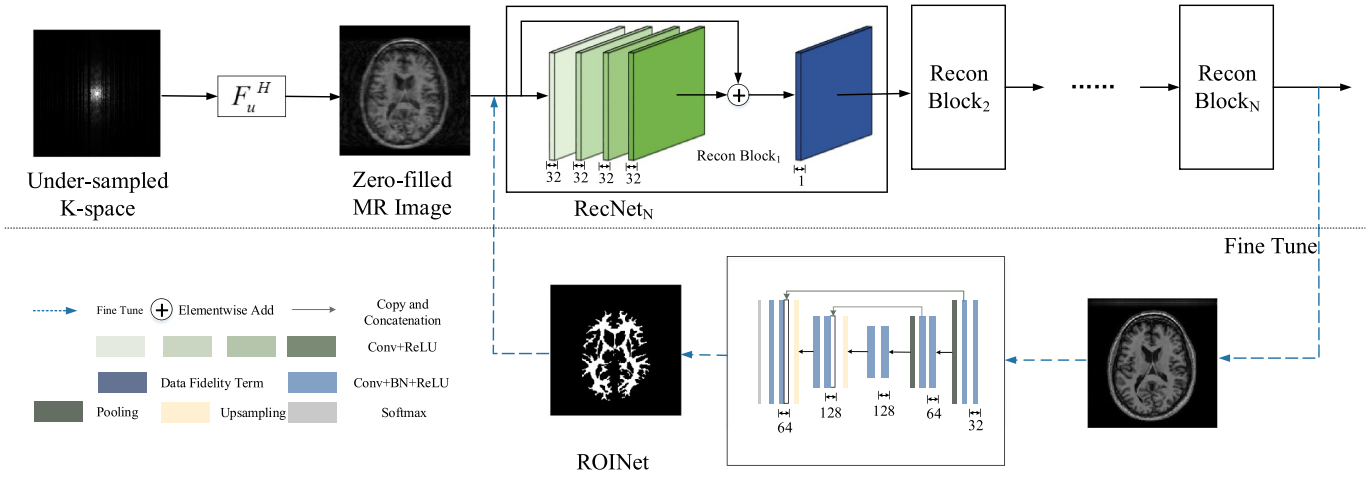

Fig. 2. The network architecture of a Region-of-Interest Reconstruction Network (ROIRecNet) for undersampled MRI reconstruction. A reconstruction network (RecNet) interpolates missing k-space values, while the ROI network focuses the reconstruction on regions of interest. These regions are determined using segmented training data for a particular region (e.g., white matter of the brain), and so ROINet is essentially a segmentation model. The parameters of RecNet are tuned to optimize over the ROI as guided by the segmentation model.

called (ROINet) with fully-sampled MRI and their corresponding segmentation labels as training data. The MRI output by RecNet are input into the ROINet to obtain the ROI masks. Then RecNet is fine-tuned using a binary weighted ℓ_2 loss function to focus on the reconstruction of the ROI. We focus on brain MRI, where the ROI can be categorized as white matter (WM), gray matter (GM) and cerebrospinal fluid (CSF). Each tissue represents a different functional region within the human brain.

2. Method

The proposed ROIRecNet model consists of a reconstruction network (RecNet) and a region-of-interest network (ROINet). Fig. 2 shows the outline of the system. For implementation, we first pre-train RecNet and ROINet, and the segmentation mask provided by ROINet is then used to further fine tune RecNet. A binary weighted ℓ_2 loss is proposed to force the network to focus on the ROI. We first describe RecNet and ROINet, and then we discuss how they are combined to form the resulting ROIRecNet architecture.

2.1. RecNet

Compared with conventional undersampled MRI reconstruction methods based on sparse representations, deep neural networks provide larger modeling capacity that can potentially represent complex MRI better, thus achieving higher reconstruction accuracy. In addition, sparsely-regularized CS-MRI methods often require heavy optimization on new MRI, resulting in slow reconstruction speed, while the MRI reconstruction models based on neural networks only use simple matrix operations requiring no iterations, so the reconstruction speed on new data is much faster.

We therefore adopt a deep neural network model for MRI reconstruction [10] based on cascaded CNNs called RecNet here. The input of the RecNet is the zero-filled MRI $F_u^H y$ obtained by padding zeros in the unsampled positions in k-space and taking an inverse 2D FFT of the Fourier coefficients. The reconstructed MRI are output to approximate the fully-sampled ground truth.

RecNet stacks four convolutional layers with a global shortcut to help stabilize training. The output of the nonlinear unit is the reconstructed MRI, but with distortions especially when the signal goes through too many layers and no corrections. Since we have accurate measurements at the sampled positions in k-space, they are used to correct the output of the nonlinear unit of each layer. In this approach, the the measured k-space values remain fixed and the reconstructed MRI produced by a nonlinear unit is transformed into the frequency domain to fill in the missing Fourier coefficients. The MRI is then reconstructed for the next layer. In Fig. 2 this is represented by the data fidelity layer. With one layer, the MRI is still low-quality, and so more "blocks" are used each having its own parameters, where the input to a block is the output of the previous block. We cascade N such blocks to form RecNet$_N$.

We pre-train RecNet$_N$ using the zero-filled and fully-sampled MRI pairs $\{F_u^H y_i, x_i^{fs}\}$ and the following ℓ_2 loss function

$$\mathcal{L}_{\text{Recon}}(y_i, x_i^{fs}; \theta_r) = \frac{1}{L_r}\sum_{i=1}^{L_r} \|x_i^{fs} - f_{\theta_r}(F_u^H y_i)\|_2^2. \tag{3}$$

Each batch contains total L_r training data pairs. The $f_{\theta_r}(\cdot)$ represents the function mapping of RecNet$_N$ with the network parameter θ_r. We will use this RecNet$_N$ model without the following ROI tuning strategy as the baseline model.

2.2. ROI extractor

In conventional ROI MRI reconstruction models, the regions of interest are determined manually in advance. But this ROI labeling by human experts can potentially be too time-consuming in practice. With the development of semantic segmentation algorithms, potential ROIs can be extracted more efficiently by automatic methods. Any automatic segmentation model can potentially be used as an ROI extractor, but more accurate segmentations can provide better guidance to the doctor. Inspired by the state-of-the-art medical image segmentation model called U-Net [21], we adopt and modify this basic architecture as an ROI extractor, which we refer to as ROINet in this context.

ROINet adopts an encoder-decoder architecture. The encoder component is used to extract features at different scales using convolution and pooling, while the decoder component is used to transform the image from feature space back to image space. We note that a shortcut method is used to feed features from lower layers to higher layers directly to reduce information loss. Batch normalization (BN) is also used to help training.

We pre-train ROINet using patches of size $\mathbb{C}^{R\times R}$ randomly cropped from fully-sampled MRI, as well as their corresponding segmentation labels as training data pairs. The cross-entropy loss function is used to train the ROINet model

$$\mathcal{L}_{\text{Seg}}(x_i^{fs}, t_i^{gt}; \theta_s) = -\sum_{i=1}^{L_s}\sum_{j=1}^{R}\sum_{c=1}^{C} t_{ijc}^{gt} \ln t_{ijc}. \tag{4}$$

The training batch contains L_s training pairs and each pixel is assigned to one of the C classes for segmentation. t^{gt} is the segmentation ground truth and t is the output of ROINet.

2.3. The ROIRecNet architecture

The pre-trained RecNet$_N$ and ROINet described above are used as building blocks for our proposed ROIRecNet architecture, which we show in Fig. 2. The under-sampled k-space measurements in the training datasets are fed into the pre-trained RecNet$_N$ to obtain an intermediate reconstruction for the MRI. Then this reconstruction is sent to the pre-trained ROINet to yield the binary mask $M \in \mathbb{R}^{P\times P}$ (in diagonal form since we are working in vectorized space) for a certain tissue of interest. On the diagonal of the mask M, the value is one for the ROI and zero otherwise. As we will see, the desired ROI will have to be only abstractly defined in advance; e.g., "white matter" could be the ROI and the ROINet model for white matter would be used.

We propose the following binary weighted ℓ_2 loss function to fine-tune the RecNet$_N$,

$$\mathcal{L}_{\text{Fitu}}(y_i, x_i^{fs}; \theta_f) = \frac{1}{L_f}\sum_{i=1}^{L_f} \|M(x_i^{fs} - f_\theta(F_u^H y_i))\|_2^2. \tag{5}$$

The training data $\{F_u^H y_i, x_i^{fs}, t_i^{gt}\}$ is used for pre-training RecNet$_N$, ROINet and fine-tuning the RecNet$_N$, while ROINet is trained using patches and RecNet is pre-trained and then fine-tuned using images. No fine-tuning is done for ROINet. The resulting network architecture is called ROIRecNet$_N$, and only the regions of interest of mask M are updated during the fine-tuning. The high-level semantic information from the segmentation network can guide the reconstruction to focus on the ROI. Note the aim for the pre-training of the RecNet$_N$ is to provide relatively clean input to the ROINet to obtain the segmentation close to the manual label. Compared with the entire image, ROIs usually contain less variation, which can significantly simplify the function mapping of the deep network. As we will show in later experiments, fewer errors in ROI at the expense of more errors in the uninteresting regions can result from this approach.

3. Experiments

3.1. Implementation details

All deep models are implemented on TensorFlow for the Python environment on a NVIDIA Geforce GTX 1080Ti with 11GB GPU memory and Intel Xeon CPU E5-2683 at 2.00 GHz. The 3×3 convolution kernel with unit stepsize is used and necessary padding is used to keep the size of input and output the same.

For the architecture in RecNet$_N$, in each block, we obtain 32 feature maps in the intermediate convolution layers and the last convolution layer outputs a single feature map of the same size as the input image. ReLU is used as activation function except for the last convolution layer within each block, where no activation is used. We use Xavier initialization for pre-training of RecNet$_N$ and ROINet. The ROINet is pre-trained for $30K$ iterations using 64×64 fully-sampled patches and their segmentation labels randomly cropped ($L_s = 16$ in a batch) and RecNet$_N$ is pre-trained on $60K$ iterations using the whole training image ($L_r = 4$ in a batch). We fine-tune RecNet$_N$ model for a further $1.2K$ iterations using the whole image ($L_f = 4$ in a batch). We select the initial learning rate to be 0.0005, the first-order momentum to be 0.9 and the second momentum to be 0.999 for pre-training. We decrease the learning rate using ADAM ten times every 4000 iterations including the fine-tune stage.

3.2. Dataset

We test the proposed architecture on the MRBrainS dataset from the Grand Challenge on MR Brain Image Segmentation workshop [22]. We use the T1 MRI data of that set having size 240×240. For the leave-one-out validation, we use three dataset for training (total of 172 slices) and a dataset for testing (total of 37 slices). We adopt the same data augmentation technique as in [23].

3.3. Results

In this section, we test the proposed ROIRecNet$_N$ model on the Brain MRI data with gray matter (GM), white matter (WM) and cerebrospinal fluid (CSF) as region-of-interest respectively. We denote GWC to be the union of these three regions. For quantitative evaluation we use peak signal-to-noise ratio (PSNR) and structural similarity index (SSIM).[1] We compare the proposed ROIRecNet model with other state-of-the-art CS-MRI models including transform learning MRI (TLMRI) [8], patch-based nonlocal operator (PANO) [24], graph-based redundant wavelet transform(GBRWT) [7] and RecNet$_4$, which shares the same architecture with deep cascaded CNN (DC-CNN) [10] and is used as the baseline here without considering ROI. The ROIRecNet$_N$ model trained on specific ROI is denoted as ROI-ROIRecNet$_N$, for example, WM-ROIRecNet$_N$ for white matter. We use a 20% 1D Cartesian under-sampling mask.

Table 1 shows quantitative performance. The deep learning architecture baseline RecNet$_N$ outperforms the state-of-the-art sparsity-based CS-MRI models as a result of the effectiveness of deep learning for this task. We also note that the proposed GM-ROIRecNet$_N$, WM-ROIRecNet$_N$, CSF-ROIRecNet$_N$ and GWC-ROIRecNet$_N$ achieve the optimal reconstruction accuracy isolated on their respective ROI, showing the advantage of the proposed ROI-based MRI reconstruction approach in these regions. In addition, GWC-ROIRecNet$_N$ has suboptimal performance on the ROI reconstruction of GM, WM and CSF, because the RecNet fine-tuning is not done specifically to any one region. Therefore, there is a clear difference in performance on various ROI depending on which model is trained. This again shows that our fine-tuning approach is actually tailoring the deep model to a desired ROI.

We also note that ROIRecNet$_N$ trained on either WM or GM ROI mutually benefits the other region, which is likely due to the similarity of these two tissues contrasted with the other regions. Another interesting phenomenon is that the reconstruction quality on the background regions decreases in all the ROIRecNet$_4$ models compared with the baseline RecNet$_4$. When training the ROIRecNet$_4$ on certain ROI, the network only focuses on improving the reconstruction quality of that ROI and similar tissues, while the background is less of a concern. This again shows that the global reconstruction error is reallocated during fine-tuning, i.e., more error in the background but less error in meaningful tissues.

We show reconstruction results using the tissues GM, WM and CSF as ROI in Figs. 3, 4 and 5, respectively. We also show the reconstruction error map, denoted Δ and magnified between [0 0.1] to better observe their differences. We see that ROIRecNet$_4$ has improved reconstruction performance over other methods in the respective ROI. This allows doctors to better focus their diagnosis in these regions.

3.4. Discussion

3.4.1. ROI extractor

In the proposed ROIRecNet architecture, a deep segmentation network is used as the ROI extractor, for which imperfect segmentation is inevitable. We evaluate this impact on the ideal ROI extraction by replacing the ROI produced from ROINet denoted M_{Seg} (the only real-world option since ground truth is unknown) with the manually segmented ground truth M_{GT}.

The training loss for the GT-ROI ROIRecNet model is

[1] The ground truth manual segmentation labels are used as ROI to evaluate the model performance.

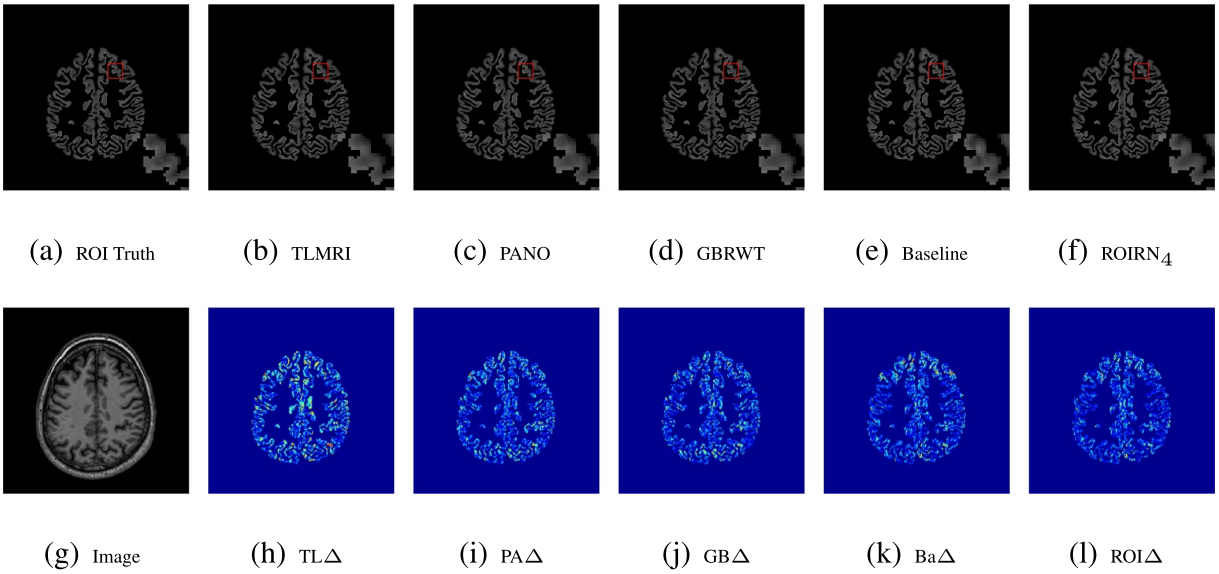

Fig. 3. The reconstructed MR images on gray matter produced by different MRI reconstruction models with reconstruction error maps.

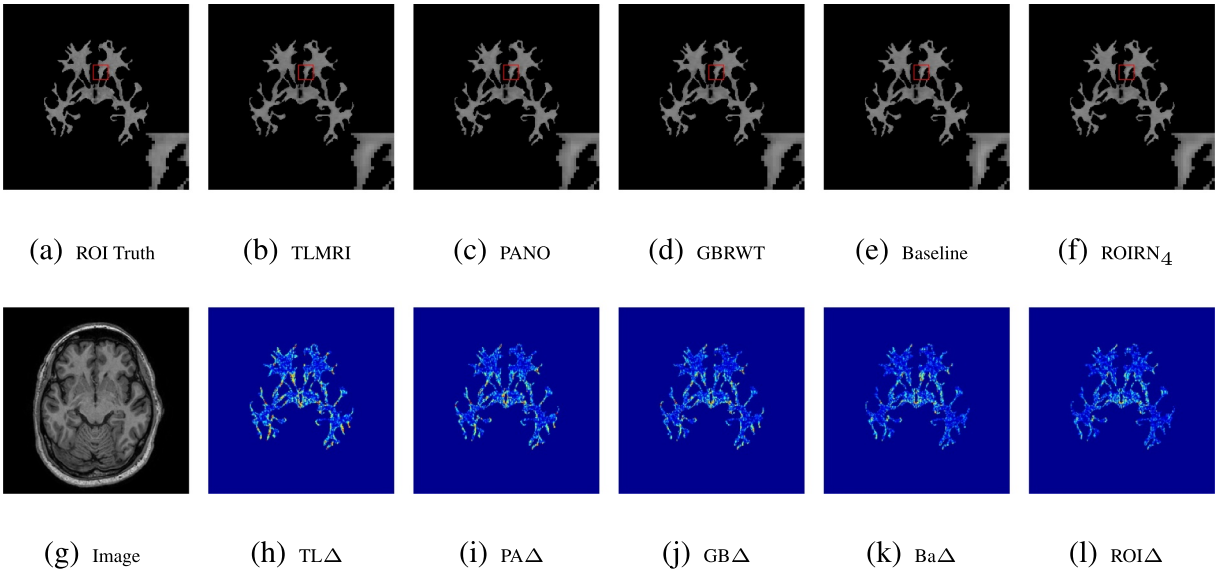

Fig. 4. The reconstructed MR images on white matter produced by different MRI reconstruction models with reconstruction error maps.

$$\mathcal{L}_{\text{Fitu}}^{\text{GT - ROI}} = \frac{1}{L_f}\sum_{i=1}^{L_f} \|M_{\text{GT}}(x_i^{fs} - f_\theta(F_u^H y_i))\|_2^2. \tag{6}$$

Correspondingly, the training loss for the Seg-ROI ROIRecNet model is

$$\mathcal{L}_{\text{Fitu}}^{\text{Seg - ROI}} = \frac{1}{L_f}\sum_{i=1}^{L_f} \|M_{\text{Seg}}(x_i^{fs} - f_\theta(F_u^H y_i))\|_2^2. \tag{7}$$

Intuitively, a better segmented ROI mask close to the groundtruth ROI mask leads to better reconstruction on the groundtruth ROI regions, and the GT-ROI ROIRecNet model can be viewed as an upperbound in ideal conditions. In Fig. 6, the experiment demonstrates that some price is being paid in the reconstruction for not knowing the ground truth segmentation.

3.4.2. Complexity of RecNet

Besides the ROI extractor, another key component of the proposed ROIRecNet$_N$ is RecNet$_N$. With more blocks, the pre-trained RecNet$_N$ can provide cleaner and clearer MRI to the ROI extractor, leading to more accurate reconstruction. We next experiment with the number of blocks N. Here, we only adopt the white matter as ROI and N ranges from 1 to 4. In Fig. 7 we see that reconstruction quality on the ROI increases with more blocks. ROIRecNet$_N$ consistently improves the baseline RecNet$_N$. This experiment shows that by adding supervision via ROINet, fewer blocks are necessary in RecNet to obtain the same performance.

3.4.3. High-frequency image details

To evaluate the impact of the ROI design on the high-frequency image details, we adopt the well-recognized metric high-frequency error norm (HFEN) to assess the reconstruction quality of high-frequency image details in sub-sampled MRI reconstruction. The HFEN metric was first proposed in the DLMRI work [25]. The HFEN metric is formulated as L2 norm of the difference of the filtered reconstructed image x^{rec} and filtered fully-sampled MR image x^{fs}

$$\text{HFEN} = \|f^{LoG} * x^{fs} - f^{LoG} * x^{rec}\|_2. \tag{8}$$

The adopted filter f^{LoG} is a Laplacian of Gaussian (LoG) filter of the size 15×15 with the standard deviation 1.5 used for extracting high frequency information. The filter parameter was set as default in [25]. A smaller

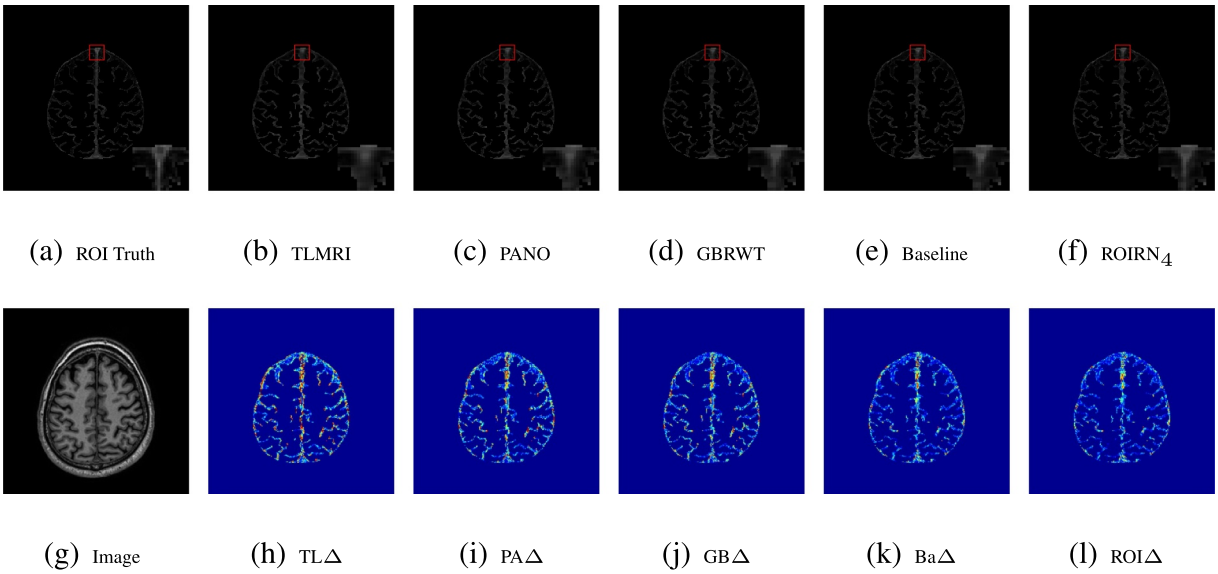

Fig. 5. The reconstructed MR images on cerebrospinal fluid produced by different MRI reconstruction models with reconstruction error maps.

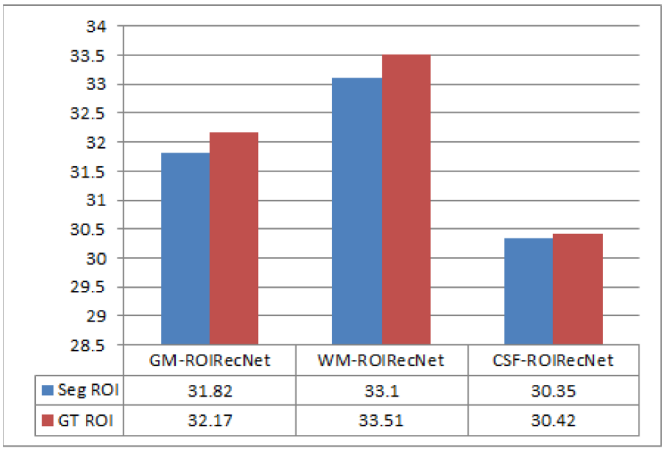

(a) PSNR dB

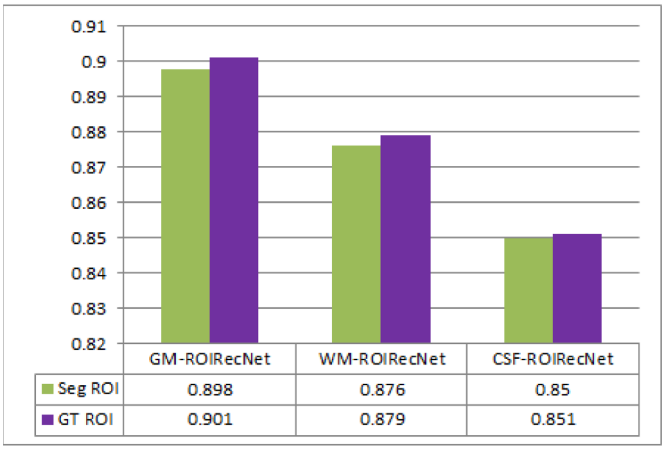

(b) SSIM

Fig. 6. The price paid for not having manual ROI segmentation by a human expert.

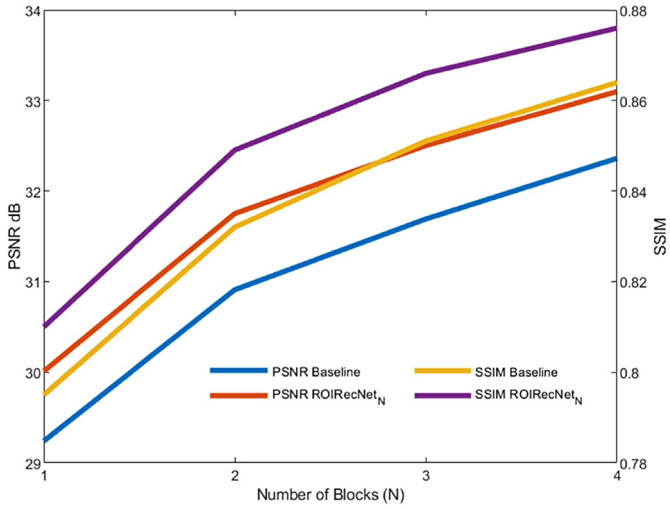

Fig. 7. Adding supervision (ROIRecNet) provides improvement over the unsupervised baseline model (RecNet) as a function of depth.

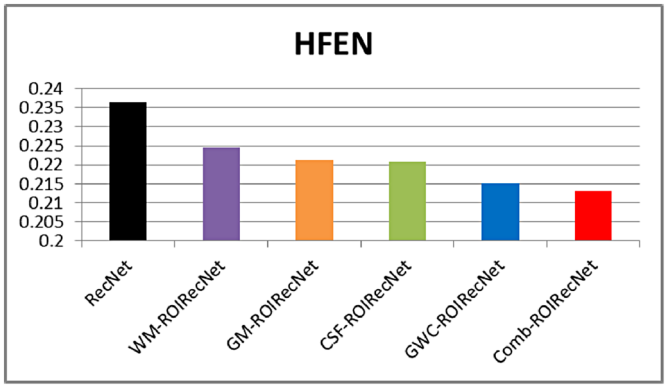

Fig. 8. The HFEN comparison among the baseline RecNet and other ROI-based models.

Table 1
The PSNR and SSIM evaluation on the ROI with compared state-of-the-art methods. The ROI is selected as gray matter (GM), white matter (WM), cerebrospinal fluid (CSF), the merge of GM, WM and CSF (GWC) and background (BG). The ROIRecNet model fine-tuned on specific ROI is also tested on other brain tissues. The

Methods	GM	WM	CSF	GWC	BG
ZF	26.50/0.785	24.76/0.735	22.35/0.599	24.56/0.749	23.87/0.450
TLMRI	29.56/0.856	29.92/0.819	26.84/0.746	28.75/0.841	29.96/0.760
PANO	30.71/0.881	31.33/0.846	28.59/0.808	30.22/0.877	31.82/0.885
GBRWT	30.99/0.883	31.64/0.853	28.81/0.814	30.50/0.882	32.25/0.930
$RecNet_4$	31.25/0.889	32.36/0.864	29.97/0.842	31.17/0.893	29.34/0.890
GM-$ROIRecNet_4$	31.82/0.898	32.68/0.872	29.92/0.840	31.41/0.895	28.41/0.855
WM-$ROIRecNet_4$	31.37/0.892	33.10/0.876	29.94/0.840	31.32/0.894	28.58/0.863
CSF-$ROIRecNet_4$	31.03/0.885	32.29/0.857	30.35/0.850	31.20/0.891	28.67/0.879
GWC-$ROIRecNet_4$	31.57/0.894	32.84/0.874	30.24/0.848	31.48/0.897	28.67/0.877

denotes the top-1 performance and the red denotes the top-2 performance.

blue

HFEN value indicates a better high-frequency reconstruction quality. We compare the basic non-ROI RecNet with all the other proposed ROI-based models in Fig. 8. The results are averaged on the test datasets used in the paper and only the whole brain regions are used in the computation. The ROI regions are generated by an automatic segmentation network. Note all the compared models here consist of 4 reconstruction blocks.

We observe that the $RecNet_4$ architecture suffers the maximum high-frequency reconstruction error, while other ROI-based models have smaller high-frequency error norms, meaning the image details at least are not deteriorated under the ROI framework.

In the reconstruction of comb-$ROIRecNet_4$, all the 3 brain tissues are targeted as ROI regions individually and then merged and combined into a final reconstruction. In such an "ensemble" ROI design, the negative effect of imperfect segmentations on edges could be reduced, thus the comb-$ROIRecNet_4$ yields the minimal error norm reasonably.

By considering the GM, WM and CSF tissues all together as a whole large ROI region, the GWC-$ROIRecNet_4$ also achieves the second-best high-frequency reconstruction accuracy. Although the results of the GM-$ROIRecNet_4$, WM-$ROIRecNet_4$ and CSF-$ROIRecNet_4$ models are worse than the comb-$ROIRecNet_4$ and GWC-$ROIRecNet_4$, the three tissue-specific ROI-based models still outperform the non-ROI $RecNet_4$, meaning we can safely implement the ROI framework without worrying about the loss of structural details outside the ROI regions compared with the baseline RecNet.

However, if the outside-ROI edges are crucial in a certain tissue-specific ROI-focused imaging task, simply implementing the GWC-ROIRecNet4 framework could help. The GWC-based ROI reconstruction is yet not as accurate as the tissue-specific ROI-based models. For example in Table 1, with regard to the reconstruction accuracy of GM

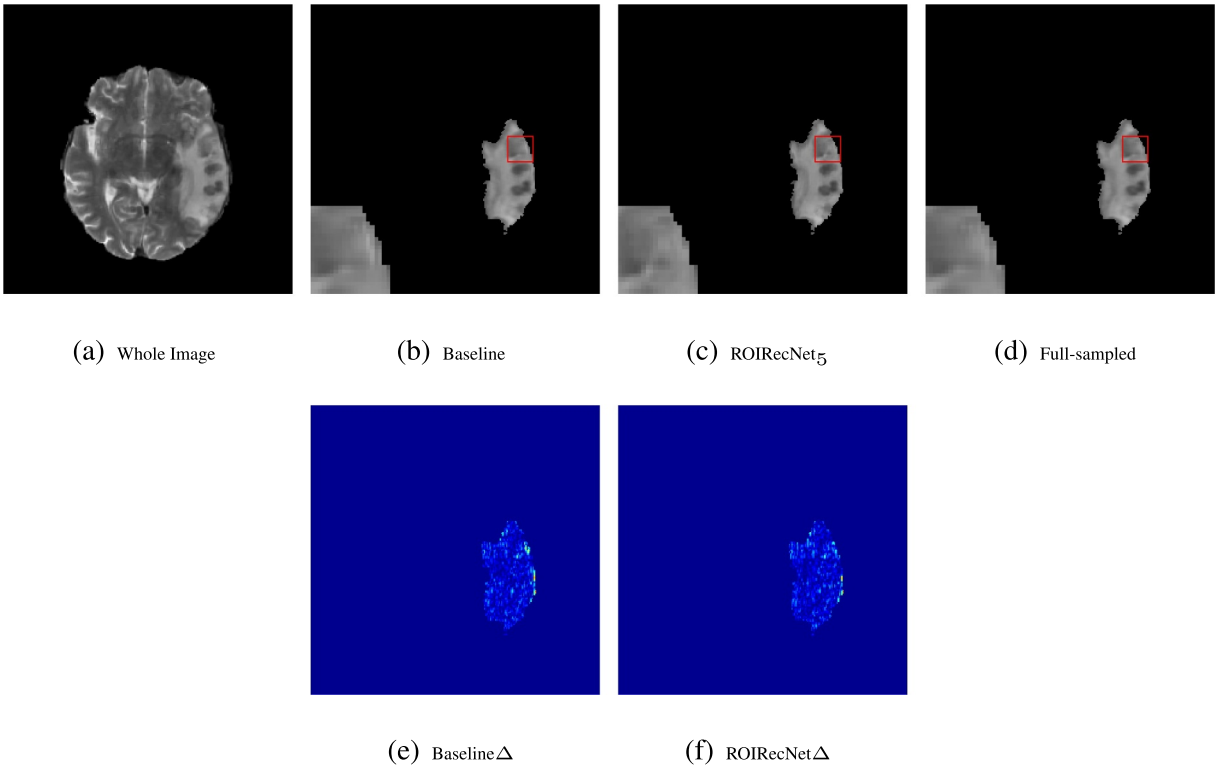

Fig. 9. The ROI MRI reconstruction of the T2 MR image on the brain tumor regions (the edema region is selected as the ROI).

tissue, we observe GM-ROIRecNet$_4$ achieves an averaged PSNR of 31.82 dB while the GWC-ROIRecNet$_4$ achieves an averaged PSNR of 31.57 dB. The comb-ROIRecNet$_4$ is also an alternative if a highly accurate edge reconstruction is desired at the cost of larger number of model parameters induced by multiple ROI networks.

3.5. Extensions: brain tumor ROI reconstruction

Since in clinics, pathology images are often of interest for radiologists, we also show an experiment of the ROIRecNet architecture on the reconstruction of MRI with brain tumors. For this experiment we use the MICCAI 2015 BRATS data [26, 27]. Here we only train and test the ROIRecNet model on the T2 weighted MRI data. For the BRATS data, the necrotic components, enhancing core, non-enhancing core and edema are manually segmented by experts. The edema region usually contains the finer pathological structures like the other 3 labeled regions. Thus we select the edema as the ROI in the extension. As shown in Fig. 9, the ROIRecNet model achieves better reconstruction accuracy on the tumor regions, thus providing more reliable diagnostic information for radiologists.

4. Conclusions

To provide more reliable MR imaging in specific tissue regions of interest, we proposed a deep neural network architecture called ROIRecNet for ROI-focused undersampled MRI reconstruction. Unlike previous methods for ROI CS-MRI, we automatically extract ROI regions using a deep segmentation network. Through fine-tuning, the reconstruction network can then provide better quality reconstructions on the ROI.

Acknowledgments

This work was supported in part by the National Natural Science Foundation of China under Grants 61571382, 81671766, 61571005, 81671674, 61671309 and U1605252, in part by the Fundamental Research Funds for the Central Universities under Grant 20720160075, 20720180059, in part by the CCF-Tencent open fund, and the Natural Science Foundation of Fujian Province of China (No. 2017J01126). L. Sun conducted portions of this work at Columbia University under China Scholarship Council grant (No. 201806310090).

References

[1] Lustig M, Donoho D, Pauly JM. Sparse MRI: the application of compressed sensing for rapid MR imaging. Magn Reson Med 2007;58(6):1182–95.
[2] Candès EJ, Romberg J, Tao T. Robust uncertainty principles: exact signal reconstruction from highly incomplete frequency information. IEEE Trans Inf Theory 2006;52(2):489–509.
[3] Fessler JA. Medical image reconstruction: a brief overview of past milestones and future directions. arXiv preprint arXiv:170705927 2017.
[4] Huang J, Zhang S, Metaxas D. Efficient MR image reconstruction for compressed MR imaging. Med Image Anal 2011;15(5):670–9.
[5] Wang S, Su Z, Ying L, Peng X, Zhu S, Liang F, et al. Accelerating magnetic resonance imaging via deep learning. ISBI. IEEE; 2016. p. 514–7.
[6] Lee D, Yoo J, Ye JC. Deep residual learning for compressed sensing MRI. ISBI. IEEE; 2017. p. 15–8.
[7] Lai Z, Qu X, Liu Y, Guo D, Ye J, Zhan Z, et al. Image reconstruction of compressed sensing MRI using graph-based redundant wavelet transform. Med Image Anal 2016;27:93–104.
[8] Ravishankar S, Bresler Y. Efficient blind compressed sensing using sparsifying transforms with convergence guarantees and application to magnetic resonance imaging. SIAM J Imag Sci 2015;8(4):2519–57.
[9] Huang Y, Paisley J, Lin Q, Ding X, Fu X, Zhang X-P. Bayesian nonparametric dictionary learning for compressed sensing MRI. IEEE Trans Image Process 2014;23(12):5007–19.
[10] Schlemper J, Caballero J, Hajnal JV, Price A, Rueckert D. A deep cascade of convolutional neural networks for MR image reconstruction. IPMI. Springer; 2017. p. 647–58.
[11] Sanfilipo MP, Benedict RH, Weinstock-Guttman B, Bakshi R. Gray and white matter brain atrophy and neuropsychological impairment in multiple sclerosis. Neurology 2006;66(5):685–92.
[12] Konar AS, Divyaa JA, Tabassum S, Sundaresan R, Czum J, Gimi B, et al. Region of interest compressed sensing MRI. J Indian Inst Sci 2014;94(4):407–14.
[13] Ilicak E, Cetin S, Bulut E, Oguz KK, Saritas EU, Unal G, et al. Targeted vessel reconstruction in non-contrast-enhanced steady-state free precession angiography. NMR Biomed 2016;29(5):532–44.
[14] Zhang C, van de Giessen M, Eisemann E, Vilanova A. User-guided compressed sensing for magnetic resonance angiography. EMBC. IEEE; 2014. p. 2416–9.
[15] Oh H, Lee S. Visually weighted reconstruction of compressive sensing MRI. Magn Reson Imaging 2014;32(3):270–80.
[16] Balafar MA, Ramli AR, Saripan MI, Mashohor S. Review of brain MRI image segmentation methods. Artif Intell Rev 2010;33(3):261–74.
[17] Aljabar P, Heckemann RA, Hammers A, Hajnal JV, Rueckert D. Multi-atlas based segmentation of brain images: atlas selection and its effect on accuracy. NeuroImage 2009;46(3):726–38.
[18] Wang L, Gao Y, Shi F, Li G, Gilmore JH, Lin W, et al. LINKS: learning-based multi-source integration framework for segmentation of infant brain images. NeuroImage 2015;108:160–72.
[19] Moeskops P, Viergever MA, Mendrik AM, Vries L S de, Benders MJ, Išgum I. Automatic segmentation of MR brain images with a convolutional neural network. IEEE Trans Med Imaging 2016;35(5):1252–61.
[20] Chen H, Dou Q, Yu L, Qin J, Heng P-A. VoxResNet: deep voxelwise residual networks for brain segmentation from 3D MR images. NeuroImage 2018;170:446–55.
[21] Ronneberger O, Fischer P, Brox T. U-net: convolutional networks for biomedical image segmentation. MICCAI. Springer; 2015. p. 234–41.
[22] Mendrik AM, Vincken KL, Kuijf HJ, Breeuwer M, Bouvy WH, De Bresser J, et al. MRBrainS challenge: online evaluation framework for brain image segmentation in 3 T MRI scans. Comput Intell Neurosci 2015;2015:1.
[23] Dong H, Yang G, Liu F, Mo Y, Guo Y. Automatic brain tumor detection and segmentation using u-net based fully convolutional networks. Annual Conference on Medical Image Understanding and Analysis. Springer; 2017. p. 506–17.
[24] Qu X, Hou Y, Lam F, Guo D, Zhong J, Chen Z. Magnetic resonance image reconstruction from undersampled measurements using a patch-based nonlocal operator. Med. Image Anal. 2014;18(6):843–56.
[25] Ravishankar S, Bresler Y. MR image reconstruction from highly undersampled k-space data by dictionary learning. IEEE Trans Med Imaging 2010;30(5):1028–41.
[26] Menze BH, Jakab A, Bauer S, Kalpathy-Cramer J, Farahani K, Kirby J, et al. The multimodal brain tumor image segmentation benchmark (BRATS). IEEE Trans Med Imaging 2015;34(10):1993–2024.
[27] Bakas S, Akbari H, Sotiras A, Bilello M, Rozycki M, Kirby JS, et al. Advancing the cancer genome atlas glioma MRI collections with expert segmentation labels and radiomic features. Sci Data 2017;4:170117.